doi.org/10.36721/PJPS.2026.39.11.303.1

Xiaoshen formula delays progression of diabetic kidney disease and improves glucose and lipid metabolism: Association with the JAK/STAT pathway

Han Yang[1], Xin Wang[3], Jin-ying Chen[1], Bo Liu[3], Hao-tian Qi[1], Xiao-xia Kang[1], Wei-chen Nie[2], Rui Chen[1]* and Tao Ding[3]*

[1]School of Traditional Chinese Medicine, Changchun University of Chinese Medicine, Changchun 130117, China
[2]School of Integrated Traditional Chinese and Western Medicine, Changchun University of Chinese Medicine, Changchun 130117, China
[3]Institute of Pharmacology and Toxicology of Traditional Chinese Medicine, Jilin Academy of Chinese Medicine Sciences, Changchun 130012, China

Abstract: **Background**: DKD is a leading cause of end-stage renal disease with limited therapeutic options. **Objectives**: This study evaluated the effects of Xiaoshen Formula (XSF) on glucose/lipid metabolism and renal injury in a DKD model of mice and preliminarily explored its mechanisms involving the JAK/STAT pathway and PPARγ. **Methods**: Diabetes and early-stage DKD were established in KK-Ay mice. Successfully modeled mice were randomly assigned to preventive or therapeutic administration groups; C57BL/6J mice served as blank controls. Biochemical parameters, kidney index and renal histopathology (hematoxylin-eosin staining and transmission electron microscopy) were assessed. Renal protein expression was determined by Western blot. **Results**: Compared with blank controls, model mice exhibited increased body weight, polydipsia, polyphagia, disrupted glucose/lipid metabolism and renal injury, confirming successful modeling. Irbesartan reduced fasting blood glucose, kidney weight, organ index and renal injury. XSF-H significantly improved glucose/lipid metabolism, reduced food/water intake and kidney weight/organ index and alleviated renal injury, with overall efficacy ranking: high-dose > therapeutic > low-dose. Western blot showed lower levels of JAK2, p-STAT-6, TGF-β1, and FN, and higher levels of PPARγ in the Irbesartan and XSF groups compared with the model group. **Conclusion**: This study provides experimental evidence that XSF may delay early DKD progression. XSF ameliorates fasting blood glucose, stabilizes body weight, improves glucose/lipid metabolism and attenuates renal injury and no obvious hepatorenal toxicity under limited conditions. Findings suggest that XSF delays DKD progression may be associated with modulation of the JAK/STAT signaling pathway and inhibition of renal fibrosis.

Keywords: Chinese herbal; Diabetic nephropathies; Glucose metabolism disorders; Janus kinases; Lipid metabolism disorders

Submitted on 23-03-2026 – Revised on 28-04-2026 – Accepted on 25-05-2026

INTRODUCTION

DM is a critical global health challenge in the 21st century. According to the IDF Diabetes Atlas (Genitsaridi *et al*., 2025), the worldwide prevalence of diabetes is projected to rise to more than 800 million by 2050. DKD, a microvascular complication of DM (Francis *et al*., 2024), often leading to end-stage renal disease (ESRD). Current standard care involves glycemic control and Renin-Angiotensin System (RAS) inhibitors (Zhang *et al*., 2020). Although SGLT2 inhibitors and GLP-1 receptor agonists show renoprotective benefits (Spasovski *et al*., 2014), they cannot halt or reverse renal fibrosis (Wehbe *et al*., 2025). Therefore, more effective therapies are urgently needed.

TCM offers multi-target advantages with favorable safety profiles. Xiaoshen Formula (XSF), derived from the academic insights of Academician Tong Xiaolin and the clinical expertise of TCM Master Nan Zheng, has been used clinically for over a decade and has induced remission in some early-stage DKD patients. Preliminary studies have partially elucidated its mechanism in retarding DKD progression. However, the effect of XSF on early DKD has not been experimentally evaluated and no previous study has directly compared its preventive and therapeutic regimens.

The JAK/STAT signaling pathway, a ubiquitous intracellular cascade, plays a pivotal role in inflammation and fibrosis (Hu *et al*., 2021). It activates classic inflammatory pathways such as NF-κB and PI3K/AKT (Zhu *et al*., 2025; Xu *et al*., 2025) and is itself activated by inflammatory mediators in DKD (Lin *et al*., 2025), underscoring its close association with disease progression.

DKD progression is driven by renal fibrosis resulting from chronic inflammation, oxidative stress and podocyte injury secondary to abnormal glucose and lipid

**Corresponding author:* e-mail: 794558014@qq.com; dtdingtao@163.com

metabolism (Guo *et al*., 2025). The JAK/STAT pathway is activated under hyperglycemia, oxidative stress and inflammation. Meanwhile, PPAR family proteins regulate lipid homeostasis (Jayaraman *et al*., 2021). Growing evidence (Jin *et al*., 2025; Li *et al*., 2022) indicates that pharmacological modulation of JAK/STAT attenuates hyperglycemia-induced renal inflammation and fibrosis, positioning this pathway as a promising therapeutic target.

In this study, diabetic and early-stage DKD models were established in KK-Ay mice and allocated to preventive and therapeutic intervention groups. The efficacy of XSF in improving glucose/lipid metabolism and retarding renal fibrosis was compared between the two regimens, and its modulation of the JAK/STAT pathway and PPAR-related protein expression was examined. It was hypothesized that XSF improves metabolic and renal outcomes through the JAK/STAT signaling pathway and PPARγ. This work was performed to elucidate the scientific basis of XSF and to provide experimental support for its potential as a TCM-based therapeutic strategy for DKD.

MATERIALS AND METHODS

Drugs

Chinese herbal compound: XSF was provided as a dry extract powder. Its main herbal constituents include Huanglian (*Coptis chinensis*), Zhimu (*Anemarrhena asphodeloides*), Chishao (*Paeonia lactiflora*), Tianhuafen (*Trichosanthes kirilowii*), Tangshuizhi (*Whitmania pigra* or *Hirudo nipponica*), Jiudahuang (*Rheum palmatum* processed with wine), Jinyingzi (*Rosa laevigata*), Qianshi (*Euryale ferox*), Danshen (*Salvia miltiorrhiza*), Huangqi (*Astragalus membranaceus*). All were purchased from the Affiliated Hospital of Changchun University of Chinese Medicine. The extract was prepared at the Drug Center of the Affiliated Hospital of Changchun University of Chinese Medicine under batch No. 20240306. Briefly, the herbs were decocted twice with 8 volumes of water for 1.5 h each time, under reduced pressure, to obtain a concentrated extract, which was then dried. Approximately 80 g of dry extract powder can be obtained from 459 g of crude drug.

Positive control drug: Irbesartan tablets (APROVEL®) were obtained from Sanofi Winthrop Industrie (approval no. H20040494; batch No. DHG1127).

Experimental animals

A total of seventy-five KK-Ay mice and twenty C57BL/6J mice (male, 6-8 weeks old, specific pathogen-free grade) were obtained from Beijing HuaFuKang Bioscience Co., Ltd. All animals were maintained under SPF conditions at the animal facility of Jilin Provincial Academy of Traditional Chinese Medicine, free access to food and water. The housing environment was controlled at 23±3°C, 40±10% relative humidity, and a light/dark cycle.

Modeling method and success criteria

Diabetes and its complications in KK-Ay mice were induced by continuous feeding of a designated high-sucrose/high-fat diet. Following one week of acclimatization, random blood glucose was measured. The diabetes model was considered successfully established if RBG exceeded 13.3 mmol/L. Subsequently, UACR was monitored periodically. An early DKD model was considered successful when UACR remained above 30 mg/g.

Administration, grouping and sample collection

The mice were allocated into two main cohorts based on the timing of intervention: a preventive administration group (Qu *et al*., 2025) and a therapeutic administration group (Liu *et al*., 2024). All mice were randomly assigned to different groups using a random number table. The specific grouping scheme, drug dosages and intervention protocols are detailed in Fig. 1 and Supplementary Materials table 1. XSF doses were expressed as grams of crude herbal material weight per kilogram, based on a pilot dose-response experiment and clinical equivalence conversion. Specifically, all drug solutions were prepared with distilled water, daily fixed-time administration. The positive drug irbesartan is administered at a daily dose of 64 mg/kg; the XSF-H dose is derived from the clinical dose, corresponding to 93.5 g/kg; while XSF-L represents half of the clinical dose, i.e., 46.75 g/kg. The model and blank control groups received an equivalent volume of distilled water by oral gavage, serving as the vehicle control. The blood glucose levels in some model mice exceeded the detection upper limit (>33.3 mmol/L) and were recorded as 33.3 mmol/L. Upon completion of the 8-week intervention period and after an 8-hour fast (free to water), all mice were anesthetized with an intraperitoneal injection of pentobarbital sodium. Blood samples were collected and kidneys were promptly excised. Renal tissues were processed for various analyses: tissues were fixed in 4% formalin at room temperature for histopathology; tissues were fixed in 2.5% glutaraldehyde and stored at 4°C for ultrastructural examination; remaining tissues were stored at -80°C in cryotubes for other analyses. Due to unexpected mortality (e.g., hyperglycemia-related death or infection) during the 8-week experiment, final group sizes varied slightly, but all exceeded 6 animals per group. The exact numbers for each group are provided in Fig. S1 and the supplementary materials. All animals that survived until the end of the experiment were included in the analysis.

Biochemical analysis

All biochemical parameters were performed according to the manufacturers' instructions. Blood samples were allowed to clot, then centrifuged to collect serum.

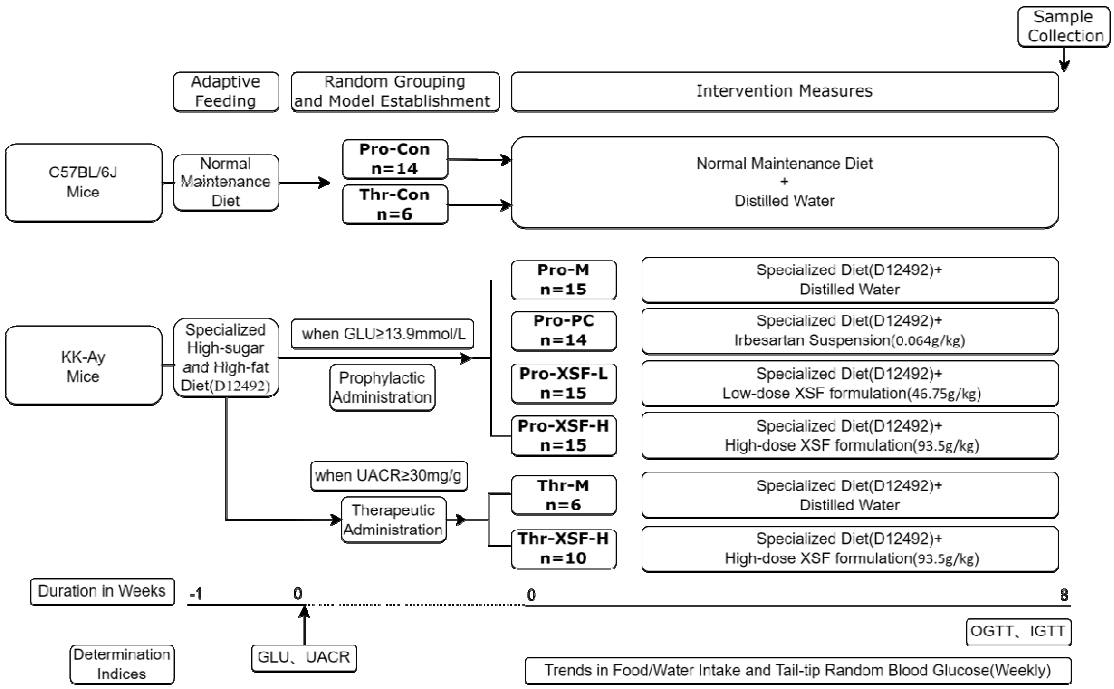

Fig. 1: Intervention flow chart.

Serum levels of biochemical indicators pertaining to glucose and lipid metabolism, renal function and liver function tests using microplate assay kits (from Nanjing Jiancheng Bioengineering Institute, China). Similarly, urine samples were centrifuged to collect the supernatant, and relevant parameters were measured using the corresponding microplate kits. All outcome assessments were performed by investigators blinded to the group allocation.

Histopathological examination

Formalin-fixed renal tissues were processed through a standardized process, then stained with H and E. Performed at 400× magnification. Histopathological evaluation was performed in a blinded manner (the examiner was unaware of group allocation). Two independent investigators reviewed all sections and reached consistent conclusions.

TEM

Renal tissues fixed in 2.5% glutaraldehyde were sliced using a standardized process, and the ultrastructural morphology of renal cells and organelles was examined under TEM (Wang *et al*., 2025). Evaluation was performed in a blinded manner (the examiner was unaware of group allocation).

Western blot analysis

All experimental steps were carried out in accordance with the standard protocols supplied by the instrument and reagent manufacturers. Renal tissues were homogenized using RIPA buffer(Jiangsu Kangwei, China). Collect the supernatant, and determine BCA by heating and separating denatured protein samples mixed with loading buffer by SDS-PAGE. Subsequently, proteins were transferred onto PVDF membranes and blocked. Membranes incubated overnight with primary antibodies (purchased from Santa Cruz Biotechnology, USA; detailed information is provided in Supplementary Material). Then incubated with secondary antibodies. Protein bands were visualized using Guangzhou Biolight (China). Intensity was quantified using ImageJ software.

Statistical analysis

Data were analyzed using GraphPad Prism software (version 8.1). Normality of distribution was assessed using the Shapiro-Wilk test and homogeneity of variances was examined using Levene's test. For comparisons among multiple groups (e.g., blank, model, positive, XSF-L, XSF-H), one-way ANOVA followed by Tukey's post-hoc test was applied. For comparisons involving two factors (e.g., time and treatment), two-way ANOVA with repeated measures was used, followed by Bonferroni's post-hoc correction. For comparisons between two independent groups (e.g., therapeutic model vs. therapeutic XSF), unpaired Student's t-test was used. All data are presented as mean ± standard error of the mean (SEM). Where applicable, 95% confidence intervals for effect sizes are reported. A P value < 0.05 was considered statistically significant.

RESULTS

Detailed numerical data, including absolute values relative to controls, are provided in Supplementary table. doc in the supplementary materials.

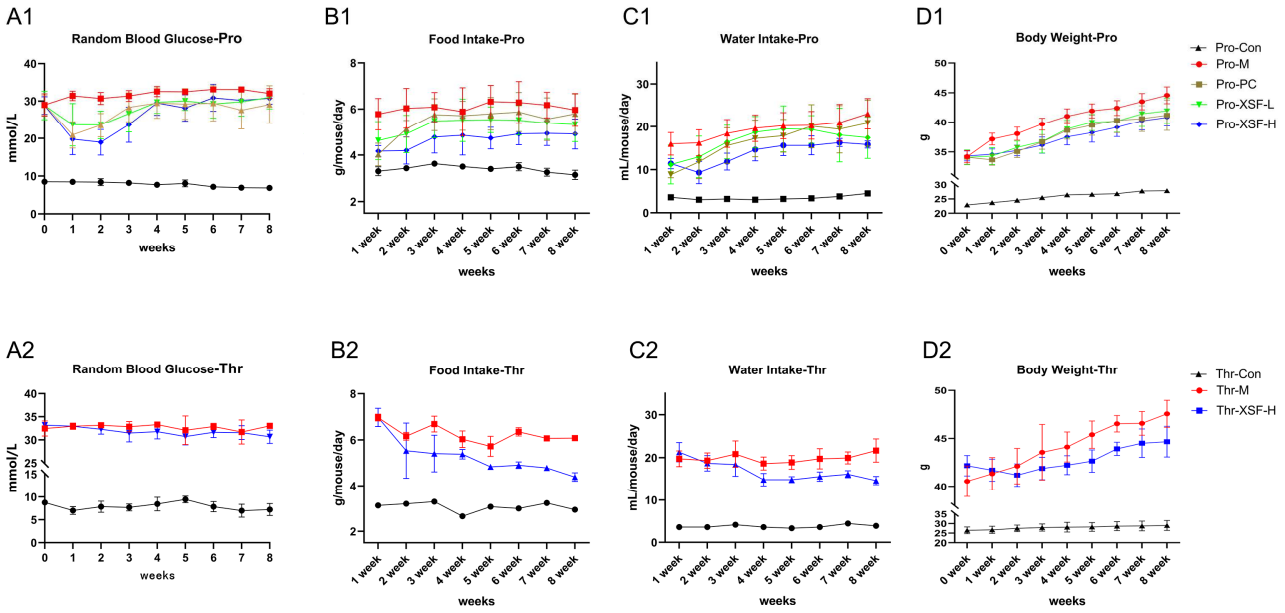

Fig. 2: Random blood glucose, food/water intake and body weight.
Note: The specific values are provided in table 2-9 of the Supplementary Materials.

XSF improves the general phenotype of diabetic KK-Ay mice

Random blood glucose: Weekly tail - tip blood glucose levels are shown in Figs 2A1 and 2A2. Compared to the blank control group, blood glucose in the model and therapeutic model groups was significantly elevated ($P < 0.001$), indicating successful hyperglycemia modeling. All preventive intervention groups effectively reduced blood glucose, and significant reductions were observed in the positive control, XSF-L, and XSF-H groups. When compared week - by - week with the model group, significant differences were found: for the positive drug at week 1, for XSF-L at weeks 1 and 2 and for XSF-H at weeks 1, 2 and 3 (all $P < 0.05$). (Fig. 2 A1 and A2).

Food intake: Weekly food consumption data are shown in Figs 2B1 and 2B2. The model and therapeutic model groups had significantly higher food intake than their respective blank controls ($P < 0.001$), consistent with the polyphagia observed in diabetic KK-Ay mice. Both XSF-L and XSF-H groups had significant reductions compared to the model group (both $P < 0.05$). The XSF therapeutic group consumed significantly less food than the therapeutic model group ($P = 0.0007$). All intervention groups had lower weekly food intake than the model group, with XSF groups having a notable effect. Week - by - week comparisons showed significant differences: for the positive drug at week 1; for XSF-L at weeks 1 and 2; for XSF-H at weeks 1–4, 5–6, 7 and 8 (all $P < 0.05$). The XSF therapeutic group had significant reductions versus the therapeutic model group at weeks 3, 6 and 8 (all $P < 0.01$) (Fig. 2.B1 /B2).

Water consumption: Figs 2C1 and 2C2 show weekly water intake. Water consumption increased significantly in the model/therapeutic model groups compared to blank controls ($P < 0.001$), consistent with the polydipsia phenotype. The XSF-H group had a significant overall reduction ($P = 0.0007$). Weekly water intake in the XSF intervention groups was lower than in the model group, and the high-dose was more effective. There were significant week - specific reductions: the positive drug at week 1; XSF-L at weeks 1 and 8; XSF-H at weeks 2, 3, 4 and 8; and the XSF therapeutic group at week 8 (all $P < 0.05$) (Fig. 2.C1/C2).

Body weight: Figs 2D1 and 2D2 show body weight changes in the preventive administration cohort. Body weight was significantly higher in the model/therapeutic model groups than in blank controls ($P < 0.001$), in line with the obesity-prone nature of the KK-Ay strain. During the intervention, the mean body weight in all drug - treated groups was lower than in the model group. There were significant reductions for the positive drug at week 1 and for the XSF-H group at weeks 3, 4, 5 ($P = 0.0466$) and 8 (all $P < 0.05$). (Fig. 2.D1/D2).

XSF ameliorates glucolipid metabolism, preserves renal function and did not induce significant changes on hepatorenal toxicity parameters

Glucose tolerance: Blood glucose profiles during the oral glucose tolerance test (GTT) are shown in Figs 3A1 and 3A2. Fasting blood glucose (FBG) was notably elevated in the model and therapeutic model groups compared to their blank controls ($P< 0.0001$), indicating sustained hyperglycemia.

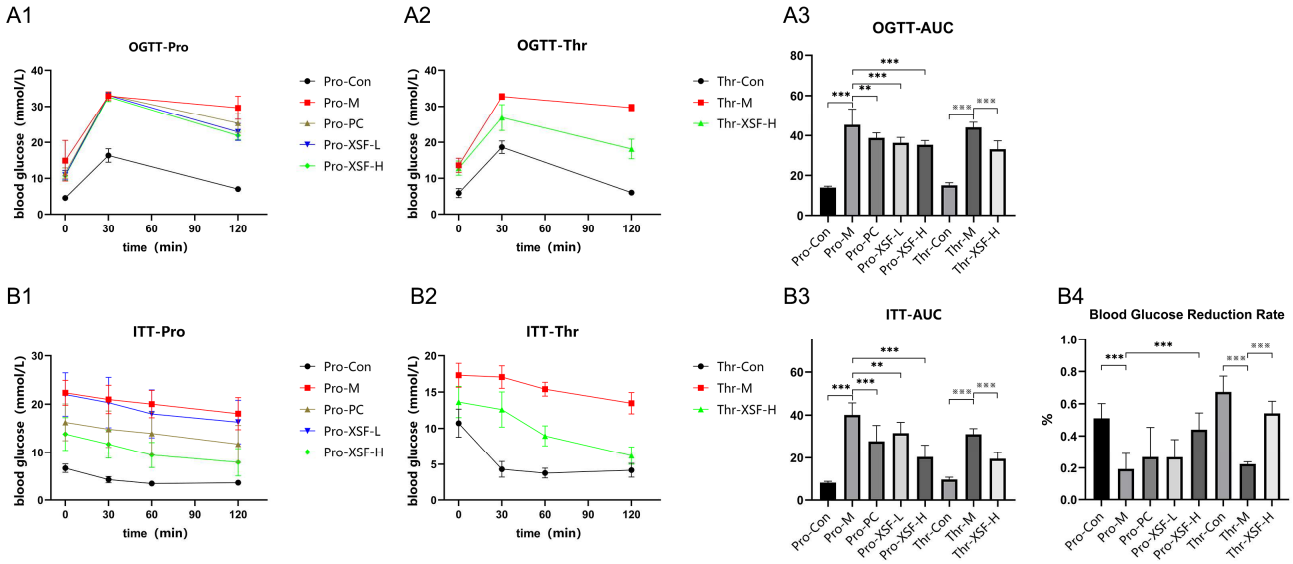

Fig. 3: Glucose tolerance test and insulin tolerance test.
Note: Compared with the model group, *: $P < 0.05$; **: $P < 0.01$; ***: $P < 0.001$.
Compared with the therapeutic model group, ※: $P < 0.05$; ※※: $P < 0.01$; ※※※: $P < 0.001$. The specific values are provided in table 10-12 of the Supplementary Materials.

All treatment groups reduced FBG levels, with significant drops in the XSF-L ($P = 0.0226$) and XSF-H ($P = 0.0049$) groups. At 30 minutes after the glucose challenge, blood glucose rose similarly in all groups, with no significant inter-group differences. However, the XSF therapeutic group had a significantly lower blood glucose level than the therapeutic model group at this time ($P < 0.0001$). By 120 minutes, blood glucose declined in all groups. Compared to the model group, glucose levels were significantly lower in the positive control ($P = 0.0037$), XSF-L ($P < 0.0001$) and XSF-H ($P < 0.0001$). The XSF therapeutic group also had a significant reduction compared to the therapeutic model group ($P < 0.0001$). The calculated area under the curve (AUC) for the GTT is presented in Fig 3A3. All drug intervention groups significantly decreased the GTT-AUC compared to the model group (positive control: $P = 0.0065$; XSF low and high dose: $P < 0.0001$). Likewise, the XSF therapeutic group had a significantly lower AUC than the therapeutic model group ($P < 0.0001$). (Fig. 3.A1/A2).

Insulin tolerance: Blood glucose changes during the ITT are shown in Figs 3B1 and 3B2. The model and therapeutic model groups had significantly higher basal blood glucose than their blank controls ($P < 0.0001$), indicating insulin resistance and successful hyperglycemia modeling. Compared to the model group, the positive drug ($P = 0.0286$) and XSF-H group ($P = 0.0002$) significantly reduced overall blood glucose during the test. All treatment groups lowered FBG compared to the model group, with the positive drug ($P = 0.0009$) and XSF-H ($P < 0.0001$) being statistically significant. After insulin injection, blood glucose decreased in all treated groups. Significant reductions were seen at 30 minutes for the positive drug (P = 0.0008) and XSF-H ($P < 0.0001$), at 60 minutes for the positive drug ($P = 0.0010$), XSF-H ($P < 0.0001$) and the XSF therapeutic group ($P = 0.0316$) and at 120 minutes for the positive drug ($P = 0.0005$), XSF-H ($P < 0.0001$) and the XSF therapeutic group ($P = 0.0046$). (Fig. 3.B1/B2).

The AUC for ITT and blood glucose decline rate are summarized in Figs 3B3 and B4 respectively. Compared with the model group, all treatment groups significantly reduced ITT-AUC (positive drug and XSF-H: $P < 0.0001$; XSF-L: $P = 0.0013$). The XSF therapeutic group had a significantly lower AUC than the therapeutic model group ($P = 0.0005$). Moreover, both the XSF-H and XSF therapeutic groups had a significantly greater blood glucose decline rate than their respective model groups ($P < 0.0001$, (Fig. 3.B3/B4).

Organ index: Kidney weight was significantly greater in the model group than in the blank control ($P < 0.0001$). All preventive treatment groups effectively lowered kidney weight compared to the model group, with the positive drug reducing it by 14.0%, XSF high dose by 16.0% (both $P < 0.0001$) and XSF low dose by 10.0% ($P = 0.0020$). In the therapeutic cohort, kidney weight was also markedly increased in the model group and was significantly reduced by XSF therapy (14.8%, $P = 0.0010$). The kidney index showed a similar trend. It increased in the model group but not significantly. However, all preventive interventions significantly reduced the kidney index compared to the model group (positive drug: 11.0% reduction, $P = 0.0023$; XSF low dose: 9.5% reduction, $P = 0.0116$; XSF high dose: 14.2% reduction, $P = 0.0001$). Similarly, the XSF therapeutic

group had a 11.9% reduction compared to the therapeutic model group (P = 0.0332). The images are in the Supplementary Materials (Supplement Fig. 1).

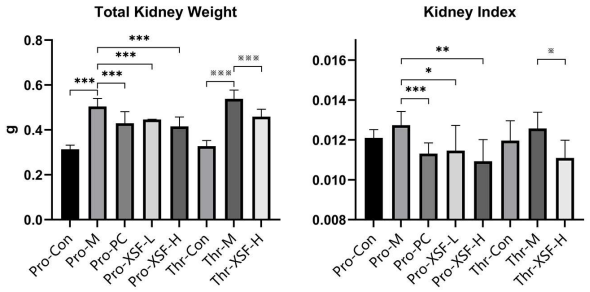

Fig. 3: Kidney Weight and Index.
Note: Compared with the model group, *: $P < 0.05$; **: $P < 0.01$; ***: $P < 0.001$. Compared with the therapeutic model group, ※: $P < 0.05$; ※※: $P < 0.01$; ※※※: $P < 0.001$.

Blood glucose and lipids: Key glucose and lipid metabolism parameters are shown in Figs 4A–F. Compared with blank controls, the model and therapeutic model groups had significantly elevated GLU, GSP, TG, TC, HDL-C, and LDL-C (all P < 0.001), indicating severe dysregulation of glucose and lipid homeostasis. The positive control drug Irbesartan significantly lowered GLU (49.8%, $P < 0.0001$) and GSP (12.5%, $P = 0.0418$). XSF-L significantly reduced GLU (26.0%, $P = 0.0112$), GSP (14.3%, $P = 0.0099$), TG (32.2%, $P < 0.0001$), TC ($P = 0.0449$) and LDL - C ($P = 0.0130$). XSF-H had more pronounced effects, significantly decreasing all measured metrics (GLU 55.6%, GSP 16.8%, TG 39.9%, TC and LDL-C all P < 0.01), but it decreased HDL-C. In the therapeutic regimen, XSF significantly reduced GLU (25.0%, $P = 0.0420$), GSP (15.0%, $P = 0.0047$), TG (17.1%, $P = 0.0011$), and LDL-C (P < 0.0001), while TC and HDL-C reductions were not statistically significant. (Figs. 4A–F).

Liver and kidney function: Hepatic and renal function markers are presented in Figs 4G–L. Compared with blank controls, the model and therapeutic model groups had significantly elevated serum levels of AST, ALT, SCr, mALB, UACR, and UCr (all P < 0.0001), indicating liver injury and renal impairment in KK-Ay mice. Irbesartan significantly lowered ALT ($P = 0.0060$), mALB ($P < 0.0001$), and UACR (54.9%; P < 0.0001), and elevated UCr ($P = 0.0280$), without significantly affecting AST or SCr. XSF-L significantly reduced AST, ALT, mALB (all $P < 0.0001$) and UACR by 47.5%. XSF-H had broader effects, significantly lowering AST ($P = 0.0003$), ALT ($P < 0.0001$), SCr ($P = 0.0002$), mALB ($P < 0.0001$) and UACR (54.9%, $P < 0.0001$). In the therapeutic regimen, XSF significantly reduced AST, ALT, SCr ($P = 0.0048$), mALB and UACR by 68.3% (all $P < 0.0001$) and increased UCr ($P = 0.0008$). XSF treatment did not cause significant changes in the assessed parameters, suggesting no obvious hepatorenal toxicity under the experimental conditions, and the high-dose regimen provided better renal protection than the positive control drug. (Figs. 4G–L).

Xiaoshen formula alleviates renal cellular pathology in KK-Ay mice

Fig. 5A shows representative photomicrographs of H & E - stained renal sections from each group. In the blank and therapeutic blank control groups, renal histology was well preserved, with normal glomeruli, regular tubular epithelial cells, minimal tubular degeneration, and scarce interstitial inflammatory cell infiltration or pathological casts, indicating normal renal histology. In contrast, the model and therapeutic model groups had marked DKD, characterized by pathological alterations such as glomerular enlargement, mesangial matrix hyperplasia, tubular degeneration, cellular casts, proteinaceous exudates, interstitial inflammatory infiltration, and fibrotic changes. Notably, all preventive and therapeutic intervention groups had significantly less renal damage than their respective model controls, as evidenced by reduced glomerular expansion and degeneration, less inflammatory cell infiltration, and overall reduced renal injury severity (Fig. 5A).

XSF attenuates glomerular basement membrane thickening and ameliorates ultrastructure

Fig. 5B shows the ultrastructural examination of glomeruli by TEM. Renal tissues from the blank and therapeutic blank control groups had normal glomerular architecture without significant hyperplasia, with uniformly arranged podocyte foot processes and an intact GBM. In contrast, specimens from the model and therapeutic model groups showed pronounced ultrastructural damage, including mesangial hyperplasia with an expanded matrix, extensive effacement of podocyte foot processes, and marked thickening of the GBM. Notably, mice treated with high-dose XSF (preventive) or XSF (therapeutic) showed significant amelioration of these pathological features. A reduction in mesangial matrix expansion showed this, decreased GBM thickness compared to their respective diabetic model groups and partial restoration of the foot process architecture (Fig. 5B).

XSF alters expression of target proteins in renal tissue

Protein expression levels of JAK2, p-STAT-6, total STAT-6, PPARγ, TGF-β1 and FN in renal tissues are shown in Fig 6. Western blot analyses were done with three biological replicates per group (n = 3), so findings are exploratory. Compared with blank controls, the model group showed higher expression of JAK2, p-STAT-6, p-STAT-6/STAT-6 ratio, PPARγ, TGF-β1, and FN, while total STAT-6 remained unchanged. In the therapeutic cohort, the model group showed increased JAK2, TGF-β1, and FN levels, with no clear differences in other factors.

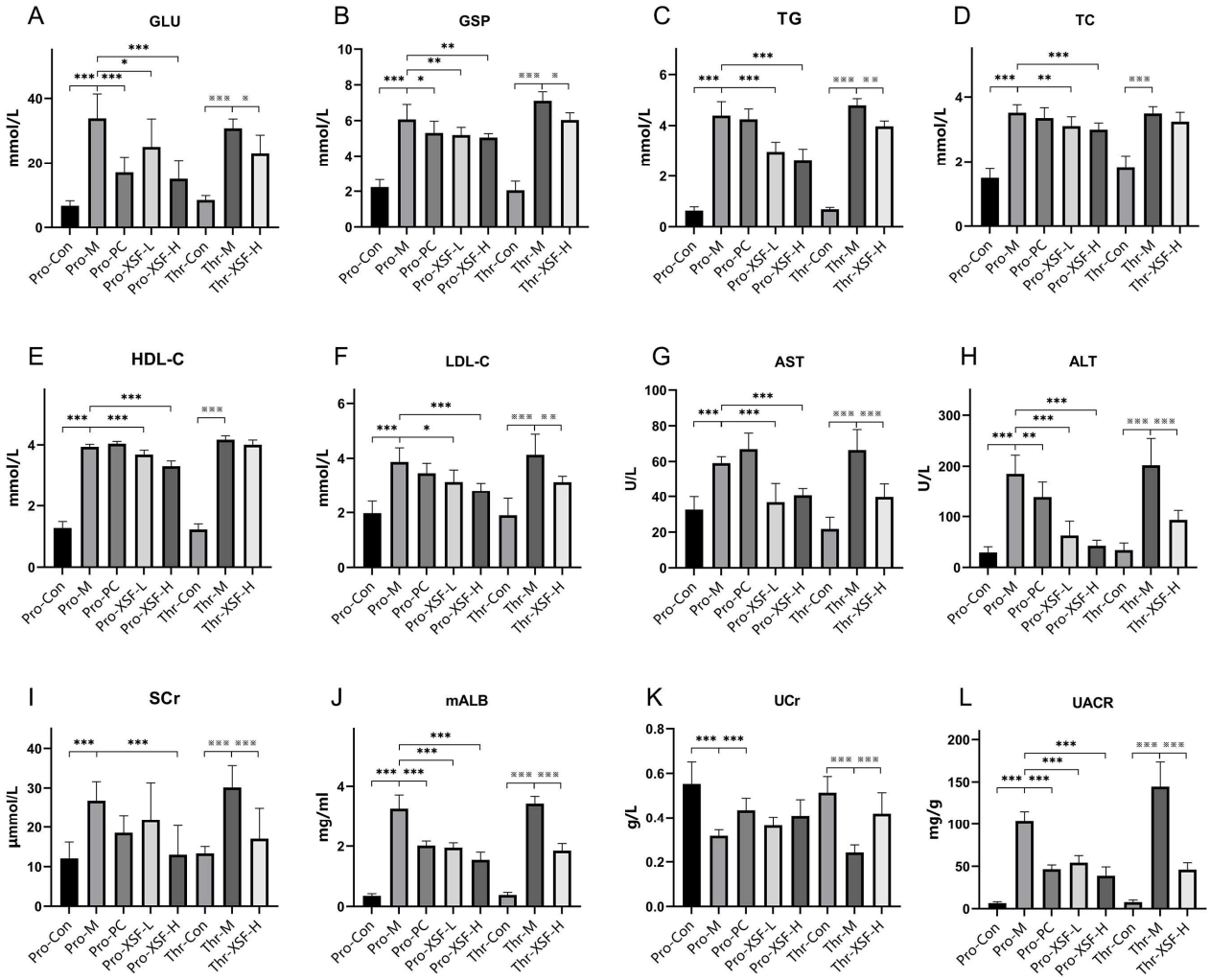

Fig. 4: Biochemical indicators.
Note: Compared with the model group, *: $P < 0.05$; **: $P < 0.01$; ***: $P < 0.001$.
Compared with the therapeutic model group, ※: $P < 0.05$; ※※: $P < 0.01$; ※※※: $P < 0.001$. The specific values are provided in Table 14-16 of the Supplementary Materials.

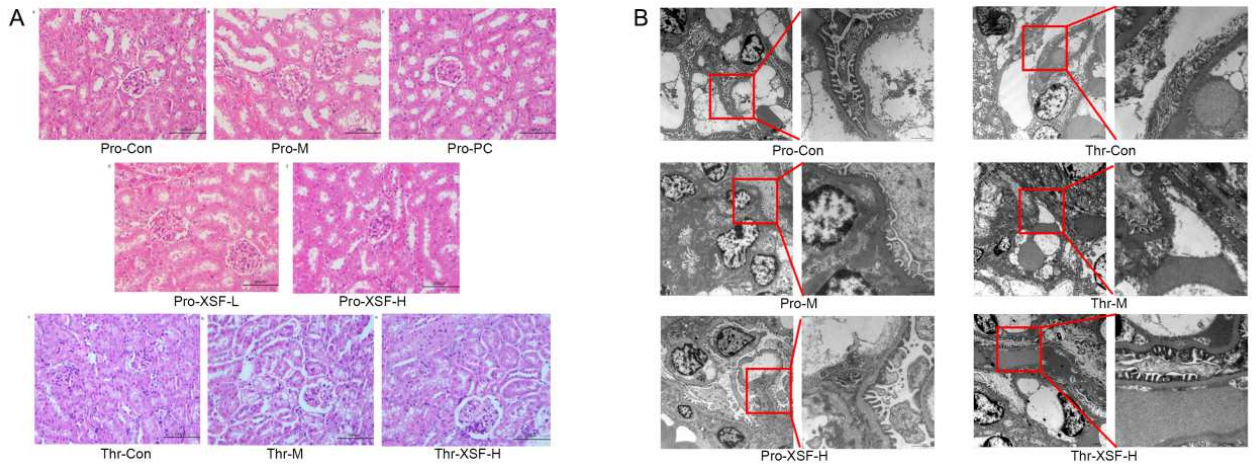

Fig. 5: Imaging changes in renal tissue of mice in each group.
(A) H & E (B) TEM

Treatment with Irbesartan trended toward downregulation of JAK2, p-STAT-6, the p-STAT-6/STAT-6 ratio and FN, and toward upregulation of PPARγ, with no consistent effect on TGF-β1 or total STAT-6. In preventive intervention, XSF-L reduced TGF-β1 and FN, while XSF-H showed more pronounced trends, lowering JAK2, p-STAT-6, the p-STAT-6/STAT-6 ratio, TGF-β1, and FN, and increasing PPARγ, with total STAT-6 unchanged. In the therapeutic regimen, XSF administration led to lower JAK2 and FN levels and higher PPARγ levels compared with the therapeutic model group, with no clear differences in other factors (Fig. 6).

DISCUSSION

The renoprotective effects of XSF, encompassing metabolic amelioration, histopathological improvement and modulation of key protein expression in KK-Ay mice with early DKD, are schematically summarized in Fig 7. It is demonstrated for the first time in a controlled comparison that XSF exerts renoprotective effects in both preventive and therapeutic settings. The observed blood glucose–lowering effect of the positive control drug Irbesartan may be attributed to its documented role in improving insulin resistance, a finding corroborated by studies (Takasu *et al*., 2006). However, the possibility that the observed metabolic benefits are partly due to reduced food intake resulting from XSF treatment cannot be excluded. Notably, the efficacy of XSF followed a clear hierarchy: preventive high-dose administration > therapeutic administration > preventive low-dose administration, indicating a distinct dose–response relationship. These metabolic changes were paralleled by decreased JAK2 and pSTAT6 expression and increased PPARγ expression, suggesting that the metabolic benefits may be linked to modulation of this pathway. This study provides in-vivo evidence supporting the potential of XSF to delay DKD progression (Fig. 7).

Prior network pharmacology analyses informed the present investigation, in which the JAK/STAT signaling pathway was highlighted as a potential target. This pathway plays a non-unidirectional role in physiological regulation. Beyond its established capacity to initiate inflammatory cascades (Du *et al*., 2021), it can itself be activated by inflammatory mediators (Banji *et al*., 2021) and by metabolic disturbances such as obesity-induced leptin dysregulation (Roh and Choi, 2023), underscoring its intimate link with abnormal lipid metabolism. This rationale guided the selection of the KK-Ay mouse model, which recapitulates hallmark features of human metabolic syndrome—including adiposity, sustained hyperglycemia, insulin resistance and islet dysfunction (Oki *et al*., 2025)—and rapidly develops DKD complications when fed a specialized diet.

JAK2, a non-receptor tyrosine kinase (Cao *et al*., 2023), phosphorylates STAT proteins, enabling their nuclear translocation and regulation of target gene transcription. STAT-6 is a key driver of type 2 immune responses (Liu *et al*., 2016) and has also been implicated in metabolic regulation (Lin *et al*., 2020). In DKD progression, sustained STAT6 activation can trigger inflammatory axes (e.g., TXNIP/NLRP3) and synergize with pro-fibrotic signals, such as TGFβ1, thereby accelerating renal fibrosis (Mossahebi-Mohammadi *et al*., 2020). Specifically, STAT6 activates bone marrow-derived fibroblasts in renal fibrosis (Yan *et al*., 2015), and its deficiency attenuates myeloid fibroblast activation and M2 macrophage polarization (Jiao *et al*., 2021). In this study, differences in the JAK/STAT axis were observed: the lowest JAK2 levels were seen in the XSF therapeutic group, followed by XSF high dose, positive drug and XSF low dose; the most pronounced decrease in p-STAT-6 was seen in the XSF high dose group, followed by positive drug, XSF therapeutic and XSF low dose. Although the literature on renal STAT6 is limited, multiple studies confirm that JAK2 and p-STAT expression are elevated in diabetic nephropathy and attenuated by herbal interventions (Hu *et al*., 2022; Ma *et al*., 2023), aligning with these findings. Unlike studies that used JAK inhibitors (e.g., AG490) or STAT6-- /- - mice, our correlative data do not establish causality.

PPARγ, a nuclear receptor pivotal in glucose and lipid homeostasis (Kielian and Drew, 2003), can synergize with STAT-6 to promote anti-inflammatory macrophage polarization (Miao *et al*., 2017) and counteract excessive extracellular matrix deposition. Its dysfunction is a central contributor to insulin resistance in type 2 diabetes (Bajaj *et al*., 2007). In this study, higher PPARγ expression was observed in the XSF high-dose group, followed by the positive drug XSF low-dose and XSF therapeutic groups. This expression trend was consistent with the superior metabolic improvements observed in the high-dose XSF group, a finding echoed in similar pharmacological studies (Ali *et al*., 2025; Rockwood *et al*., 2019). However, PPARγ expression was markedly elevated in all KK-Ay mouse groups compared to the blank C57 controls. This contrasts with some reports showing reduced PPARγ in diabetic kidney disease (Zhao *et al*., 2016; Fu *et al*., 2025). The discrepancy may be attributed to the experimental design and the selection of the animal model. KK-Ay mice were exclusively fed with a specialized high-sugar, high-fat diets, whereas C57 mice received only standard maintenance diets, resulting in completely different lipid metabolism states between two groups. Consequently, baseline PPARγ expression—a protein closely associated with lipid metabolism—differed substantially. The elevated PPARγ level in KK-Ay mice may reflect compensatory feedback mechanisms in their lipid metabolism pathways. Additionally, the metabolic decline in aged mice or inherent model variations could account for the observed differences in expression patterns.

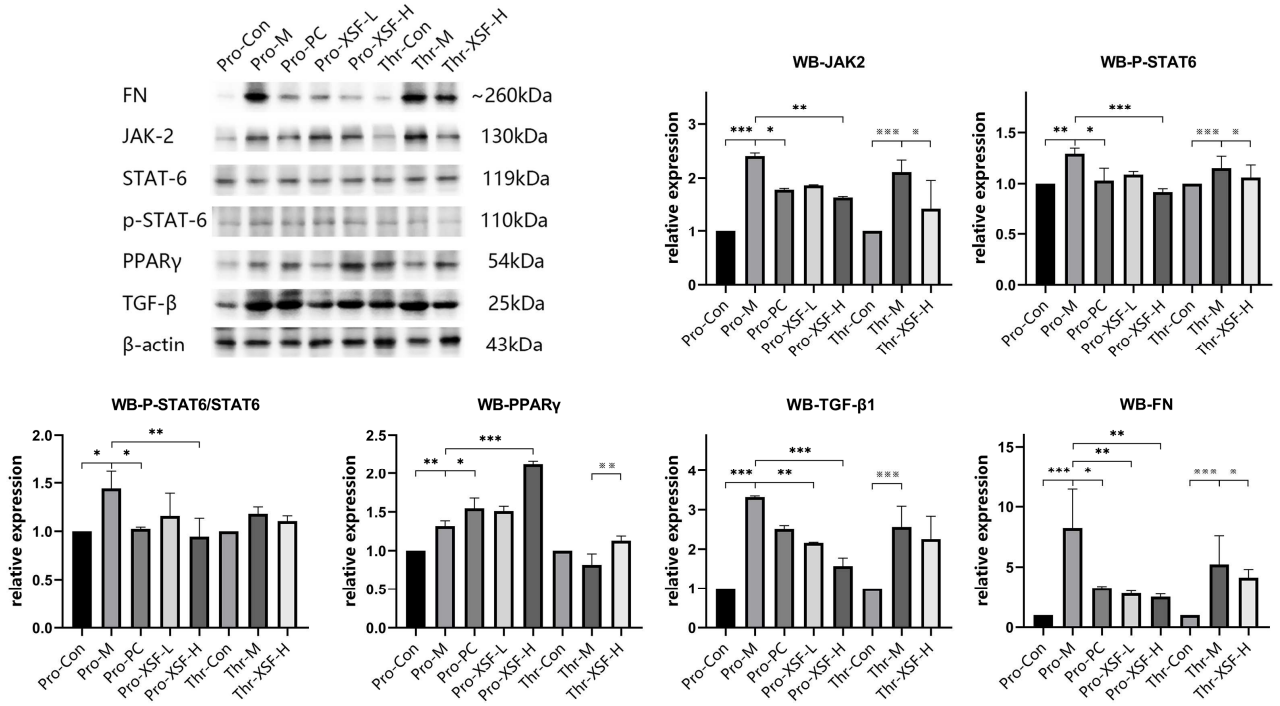

Fig. 6: Expression levels of related proteins in renal tissues of mice in each group.
Note: Vs β-actin. Preventive groups normalized to the blank group, therapeutic groups normalized to the therapeutic blank group, n=3. Compared with the model group, *: $P < 0.05$; **: $P < 0.01$; ***: $P < 0.001$.
Compared with the therapeutic model group, ※: $P < 0.05$; ※※: $P < 0.01$; ※※※: $P < 0.001$.
The specific values are provided in Table 17-18 of the Supplementary Materials.

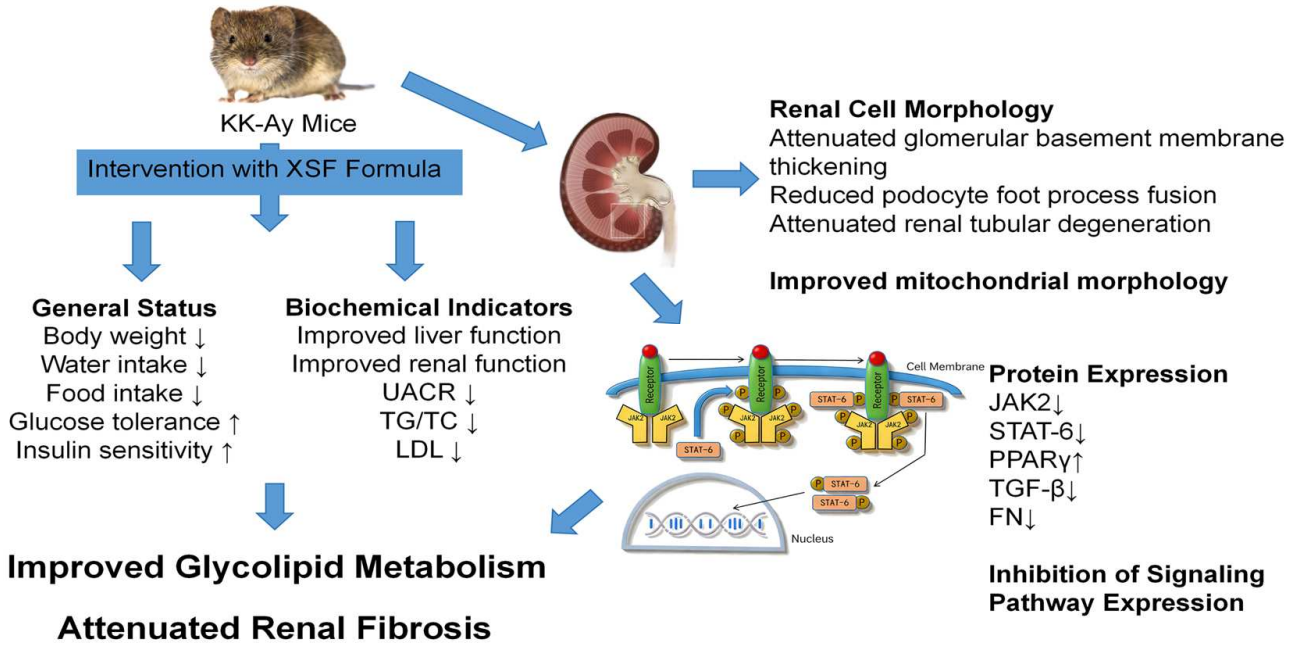

Fig. 7: Xiaoshen formula delays the progression of DKD in KK-Ay mice (Graphical Abstract).

TGF-β1 is a pleiotropic cytokine with dual roles. Its chronic activation drives excessive extracellular matrix deposition and sclerosis, leading to fibrosis (Tao *et al*., 2025). Fibronectin (FN) is a primary matrix protein deposited early in this process and serves as a direct downstream marker of TGF-β1 activity (Pan *et al*., 2024).

All treatment groups showed lower TGF-β1 expression, with the order of XSF high dose > XSF therapeutic > XSF low dose > positive drug, which may be associated with anti-fibrotic effects; however, causality is not established. This aligns with trends reported in other studies (Liao *et al*., 2021; Gao *et al*., 2014). Overall, the degree of metabolic improvement (e.g., reduction in GLU and TG) across treatment groups correlated with the extent of JAK/STAT pathway modulation and PPARγ upregulation, suggesting a potential link between metabolic regulation and signaling changes.

This research is grounded in the TCM theory of ‘spleen deficiency and kidney solidity’ in diabetic nephropathy. From a TCM perspective, renal fibrosis might be interpreted as a manifestation of ‘solidity’. Nevertheless, the experimental data only demonstrate the presence of fibrosis and its reduction by XSF; establishing a direct correspondence between TCM concepts and molecular mechanisms is beyond the scope of this study.

This study has limitations. Technical constraints during random blood glucose measurement (e.g., values exceeding glucometer range) may have compromised accuracy, potentially affecting statistical significance in later time points, However, FBG and other parameters, as well as key renal outcome indicators (UACR, UCR, pathology), remained unaffected by this factor; thus, the overall conclusions remain reliable. Due to limited toxicity assessment (no dedicated assays), the conclusion of “no hepatorenal toxicity” is restricted to this short-term study and should be interpreted cautiously. Western blot analyses were performed with only three biological replicates. The results should therefore be considered exploratory and trend-revealing rather than definitive mechanistic evidence. In addition, due to the complexity of the herbal formula, potential variability in herbal preparations, and the scope of the present study, we did not employ pathway-specific inhibitors or genetic interventions, nor was mRNA level validation (e.g., qPCR) performed. Consequently, the causal relationship between the observed modulation of the JAK/STAT pathway and PPARγ and the renoprotective effects of XSF remains to be established in future studies. Due to ongoing patent protection of the formulation ratios, full chemical characterization and mass spectrometry data are not provided here. However, the main herbal constituents, source, extraction procedure, batch number and yield have been detailed to support reproducibility. Future work will include HPLC fingerprinting for further standardization. The lack of quantitative histopathological scoring limits the objectivity of the assessment. Although the application of the blinding method and the consistency of the qualitative results still confirm the study's reliability. We also acknowledge that newer first-line DKD therapies (e.g., SGLT2 inhibitors) were not included as positive controls, the selection of a single animal model also affects the generalizability of the experiment. These also require improvement in future experiments.

JAK inhibitors are under clinical evaluation for autoimmune and metabolic diseases (Fleischmann *et al*., 2012; Wallace *et al*., 2018; Waibel *et al*., 2023). However, the pathway's bidirectional nature complicates therapeutic strategies, as its broad physiological roles mean that simple blockade may yield suboptimal or off-target effects. Increasingly, diseases are understood as disruptions in dynamic physiological networks rather than failures of linear pathways. This perspective resonates with the TCM concept of "soil-seed" relationships within Academician Tong Xiaolin's "State-Target Differentiation and Treatment" framework. The multi-target, system-regulating nature of herbal formulas like XSF may thus be particularly well-suited to modulate such complex, interconnected pathways. Exploring how herbal medicines fine-tune the JAK/STAT axis and related metabolic signals could offer novel therapeutic avenues for DKD and other diseases rooted in metabolic-inflammatory crosstalk.

CONCLUSION

The Chinese herbal compound Xiaoshen Formula (XSF) effectively mitigated multiple pathological features in a KK-Ay mouse model of DKD. XSF treatment reduced body weight, food and water intake and fasting blood glucose and improved glucose and lipid metabolism. It also provided significant renal protection, as evidenced by reduced kidney weight coefficient, alleviated histopathological damage, and attenuated glomerular basement membrane hyperplasia, which contributed to delaying DKD progression.

The underlying mechanism may involve modulation of the JAK/STAT signaling pathway and regulation of key proteins in fibrosis and metabolism, specifically lower TGF-β1 and FN expression and higher PPARγ expression. This multi-target action seems to delay the renal fibrotic process. A preventive administration regimen, especially at a high dose, was more effective than therapeutic intervention and no significant hepatorenal toxicity was observed.

These findings offer experimental evidence that XSF is a promising, multi-faceted therapeutic candidate from TCM for the clinical management of DKD.

Acknowledgments

This work was supported by the Jilin Provincial Natural Science Foundation (Grant No. YDZJ202401001ZYTS). The authors thank the Jilin Academy of Chinese Medicine Sciences for providing the experimental facilities.

AI disclosure: The authors used DeepSeek (https://www.deepseek.com) for language translation and

polishing. The purpose of using this AI tool was to improve the readability and linguistic accuracy of the manuscript.

Authors' contributions

Han Yang contributed to conceptualization, data curation, formal analysis, investigation, methodology and writing of the original draft; Xin Wang, Jin-ying Chen, Bo Liu, Hao-tian Qi, Xiao-xia Kang and Wei-chen Nie participated in investigation, methodology, validation, visualization, formal analysis, resources, software, project administration and supervision; Rui Chen and Tao Ding contributed to conceptualization, funding acquisition, project administration, supervision and writing—review and editing. All authors have read and approved the final version of the manuscript.

Funding

This work was supported by the Jilin Provincial Natural Science Foundation under Grant No. YDZJ202401001ZYTS for the project entitled "Molecular Mechanism of Xiaoshen Formula Intervention in Diabetic Kidney Disease Based on PINK1/Parkin Signaling Pathway-Mediated Mitophagy".

Data availability statement

All data generated or analysed during this study are included in this published article and its supplementary information files.

Ethical approval

All animal experiments were conducted in accordance with relevant guidelines and regulations and were reviewed and approved by the respective Experimental Animal Ethics Committees of Changchun University of Chinese Medicine (Approval No. 2024068) and the Jilin Provincial Academy of Traditional Chinese Medicine (Approval No. JLSZKYDWLL2023-020). This study was performed in adherence with the ARRIVE guidelines. See supplementary file for the ARRIVE checklist.

Conflict of interest

The authors declare no conflict of interest.

Supplementary data

REFERENCES

Kidney disease: Improving global outcomes (KDIGO) CKD Work Group, 2024. KDIGO 2024 clinical practice guideline for the evaluation and management of chronic kidney disease. *Kidney Int,* **105**(4S): S117-S314.

Ali AA, Aljumayi H, Aljutaily T, Alfheeaid HA, Al-Zunaidy NBA, Mohamed Ahmed IA, Mohammed BM and Khalil NA (2025). The hypolipemic properties of kaempferol presented in microwaved cooked broccoli between hyperlipidemic rat models. *Food Sci. Nutr.,* **13**: e70556.

Bajaj M, Suraamornkul S, Hardies LJ, Glass L, Musi N and Defronzo RA (2007). Effects of peroxisome proliferator-activated receptor (PPAR)-alpha and PPAR-gamma agonists on glucose and lipid metabolism in patients with type 2 diabetes mellitus. *Diabetologia,* **50**: 1723-31.

Banji D, Alqahtani SS, Banji OJF, Machanchery S and Shoaib A (2021). Calming the inflammatory storm in severe COVID-19 infections: Role of biologics- A narrative review. *Saudi Pharm J,* **29**: 213-222.

Cao Y, Wang J, Jiang S, Lyu M, Zhao F, Liu J, Wang M, Pei X, Zhai W, Feng X, Feng S, Han M, Xu Y and Jiang E (2023). JAK1/2 inhibitor ruxolitinib promotes the expansion and suppressive action of polymorphonuclear myeloid-derived suppressor cells via the JAK/STAT and ROS-MAPK/NF-κB signalling pathways in acute graft-versus-host disease. *Clin Transl Immunology,* **12**: e1441.

Du X, Wang X, Cui K, Chen Y, Zhang C, Yao K, Hao Y and Chen Y (2021). Tanshinone IIA and astragaloside IV inhibit miR-223/JAK2/STAT1 signalling pathway to alleviate lipopolysaccharide-induced damage in nucleus pulposus cells. *Dis Markers,* **2021**: 6554480.

Fleischmann R, Kremer J, Cush J, Schulze-Koops H, Connell CA, Bradley JD, Gruben D, Wallenstein GV, Zwillich SH and Kanik KS (2012). Placebo-controlled trial of tofacitinib monotherapy in rheumatoid arthritis. *N Engl J Med,* **367**: 495-507.

Francis A, Harhay MN, Ong ACM, Tummalapalli SL, Ortiz A, Fogo AB, Fliser D, Roy-Chaudhury P, Fontana M, Nangaku M, Wanner C, Malik C, Hradsky A, Adu D, Bavanandan S, Cusumano A, Sola L, Ulasi I and Jha V (2024). Chronic kidney disease and the global public health agenda: An international consensus. *Nat Rev Nephrol,* **20**: 473-485.

Fu Y, Zhang X, Xu R and Lv B (2025). Fisetin-mediated PPAR-γ upregulation: A novel therapeutic approach for corpus cavernosum smooth-muscle-cell apoptosis and restoration of erectile function after cavernous nerve injury. *Transl Androl Urol,* **14**: 1429-1443.

Gao C, Aqie K, Zhu J, Chen G, Xu L, Jiang L and Xu Y (2014). MG132 ameliorates kidney lesions by inhibiting the degradation of Smad7 in streptozotocin-induced diabetic nephropathy. *J Diabetes Res,* **2014**: 918396.

Genitsaridi I, Salpea P, Salim A, Sajjadi SF, Tomic D, James S, Thirunavukkarasu S, Issaka A, Chen L, Basit A, Luk AOY, Ma RCW, Mbanya JC, Ramachandran A, Wild SH, Duncan BB, Boyko EJ and Magliano DJ (2025). 11th edition of the IDF Diabetes Atlas: Global, regional and national diabetes prevalence estimates for 2024 and projections for 2050. *Lancet Diabetes Endocrinol*.

Guo M, Ni L and Wu X (2025). Natural products as potential therapeutic candidates for diabetic kidney disease: Molecular mechanisms, translational challenges and future prospects. *Int J Mol Sci,* **26**(23): 11637.

Hu X, Li J, Fu M, Zhao X and Wang W (2021). The JAK/STAT signaling pathway: From bench to clinic. *Signal Transduct Target Ther,* **6**: 402.

Hu Y, Liu S, Liu W, Zhang Z, Liu Y, Li S, Sun D, Zhang G and Fang J (2022). Potential molecular mechanism of yishen capsule in the treatment of diabetic nephropathy based on network pharmacology and molecular docking. *Diabetes Metab Syndr Obes,* **15**: 943-962.

Jayaraman S, Devarajan N, Rajagopal P, Babu S, Ganesan SK, Veeraraghavan VP, Palanisamy CP, Cui B, Periyasamy V and Chandrasekar K (2021). β-Sitosterol circumvents obesity induced inflammation and insulin resistance by down-regulating IKKβ/NF-κB and JNK signaling pathway in adipocytes of type 2 diabetic rats. *Molecules,* **26**(7): 2101.

Jiao B, An C, Du H, Tran M, Wang P, Zhou D and Wang Y (2021). STAT6 deficiency attenuates myeloid fibroblast activation and macrophage polarization in experimental folic acid nephropathy. *Cells,* **10**(11): 3057.

Jin T, Du Y, Liu C, Zhao J and Liu T (2025). Advances in ginsenoside treatment for common kidney diseases: Pharmacological evaluation and potential mechanisms. *Front Pharmacol,* **16**: 1702234.

Kielian T and Drew PD (2003). Effects of peroxisome proliferator-activated receptor-gamma agonists on central nervous system inflammation. *J Neurosci Res,* **71**: 315-25.

Li Y, Li Y, Chen N, Feng L, Gao J, Zeng N, He Z and Gong Q (2022). Icariside II exerts anti-type 2 diabetic effect by targeting PPARα/γ: Involvement of ROS/NF-κB/IRS1 signaling pathway. *Antioxidants (Basel),* **11**(9): 1705.

Liao X, Jiang Y, Dai Q, Yu Y, Zhang Y, Hu G, Meng J, Xie Y, Peng Z and Tao L (2021). Fluorofenidone attenuates renal fibrosis by inhibiting the mtROS-NLRP3 pathway in a murine model of folic acid nephropathy. *Biochem Biophys Res Commun,* **534**: 694-701.

Lin H, Yang Y, Wang X, Chung M, Zhang L, Cai S, Pan X and Pan Y (2025). Targeting the AGEs-RAGE axis: Pathogenic mechanisms and therapeutic interventions in diabetic wound healing. *Front Med (Lausanne),* **12**: 1667620.

Lin SY, Yang CP, Wang YY, Hsiao CW, Chen WY, Liao SL, Lo YL, Chang YH, Hong CJ and Chen CJ (2020). Interleukin-4 improves metabolic abnormalities in leptin-deficient and high-fat diet mice. *Int J Mol Sci,* **21**(12): 4451.

Liu L, Sun Q, Bao R, Roth M, Zhong B, Lan X, Tian J, He Q, Li D, Sun J, Yang X and Lu S (2016). Specific regulation of PRMT1 expression by PIAS1 and RKIP in BEAS-2B epithelia cells and HFL-1 fibroblasts in lung inflammation. *Sci Rep,* **6**: 21810.

Liu X, Jiang L, Zeng H, Chen Y, Wang L, Zhang H and Li W (2024). Circ-0000953 deficiency exacerbates podocyte injury and autophagy disorder by targeting Mir665-3p-Atg4b in diabetic nephropathy. *Autophagy,* **20**(5): 1072-1097.

Ma Y, Deng Y, Li N, Dong A, Li H, Chen S, Zhang S and Zhang M (2023). Network pharmacology analysis combined with experimental validation to explore the therapeutic mechanism of Schisandra Chinensis Mixture on diabetic nephropathy. *J Ethnopharmacol,* **302**: 115768.

Miao X, Leng X and Zhang Q (2017). The current state of nanoparticle-induced macrophage polarization and reprogramming research. *Int J Mol Sci,* **18**(2): 336.

Mossahebi-Mohammadi M, Quan M, Zhang JS and Li X (2020). FGF signaling pathway: A key regulator of stem cell pluripotency. *Front Cell Dev Biol,* **8**: 79.

Oki C, Uno K, Sasase T, Tsutsui T, Sekiguchi K, Yamaguchi A, Mandai K, Shinohara M, Sugimoto M, Maekawa T, Miyajima K and Ohta T (2025). High-fat/high-sucrose diet-induced renal changes in obese diabetic mice: A comparison with db/db and KK-Ay mice. *J Vet Med Sci,* **87**: 138-146.

Pan D, Qu Y, Shi C, Xu C, Zhang J, Du H and Chen X (2024). Oleanolic acid and its analogues: Promising therapeutics for kidney disease. *Chin Med,* **19**: 74.

Qu Q, Liu SY, Fu B, Zhang Q, Li J, Chen H, Wang X, Liu Y and Sun L (2025). Gingival mesenchymal stem cell-derived exosomal miR-23a-3p targets IL-6R to attenuate autoimmune insulitis: A cell-free therapeutic strategy for type 1 diabetes. *Stem Cell Res Ther,* **16**(1): 633.

Rockwood S, Mason D, Lord R, Lamar P, Prozialeck W and Al-Nakkash L (2019). Genistein diet improves body weight, serum glucose and triglyceride levels in both male and female ob/ob mice. *Diabetes Metab Syndr Obes,* **12**: 2011-2021.

Roh E and Choi KM (2023). Hormonal gut-brain signaling for the treatment of obesity. *Int J Mol Sci,* **24**(4): 3384.

Spasovski G, Vanholder R, Allolio B, Annane D, Ball S, Bichet D, Decaux G, Fenske W, Hoorn EJ, Ichai C, Joannidis M, Soupart A, Zietse R, Haller M, Van Der Veer S, Van Biesen W and Nagler E (2014). Clinical practice guideline on diagnosis and treatment of hyponatraemia. *Nephrol Dial Transplant,* **29**(Suppl 2): i1-i39.

Takasu T, Kakuta H, Sasamata M and Yamagishi S (2006). An angiotensin II (Ang II) type 1 receptor blocker, telmisartan, improves insulin resistance in KK-A(y) diabetic mice. *Int J Biomed Sci,* **2**: 333-6.

Tao X, Wu Y, Guo F, Lv L, Zhai X, Shang D, Yu Z, Xiang H and Dong D (2025). Targeted inhibitors of S100A9 alleviate chronic pancreatitis by inhibiting M2

macrophage polarization via the TAOK3-JNK signaling pathway. *Front Immunol,* **16**: 1526813.

Waibel M, Wentworth JM, So M, Couper JJ, Cameron FJ, Macisaac RJ, Atlas G, Gorelik A, Litwak S, Sanz-Villanueva L, Trivedi P, Ahmed S, Martin FJ, Doyle ME, Harbison JE, Hall C, Krishnamurthy B, Colman PG, Harrison LC, Thomas HE and Kay TWH (2023). Baricitinib and β-cell function in patients with new-onset type 1 diabetes. *N Engl J Med,* **389**: 2140-2150.

Wallace DJ, Furie RA, Tanaka Y, Kalunian KC, Mosca M, Petri MA, Dorner T, Cardiel MH, Bruce IN, Gomez E, Carmack T, Delozier AM, Janes JM, Linnik MD, De Bono S, Silk ME and Hoffman RW (2018). Baricitinib for systemic lupus erythematosus: A double-blind, randomised, placebo-controlled, phase 2 trial. *Lancet,* **392**: 222-231.

Wehbe F, Elliott M and Levin A (2025). CKDs at the crossroads: From failures to future therapies. *Kidney Int Rep,* **10**: 4145-4161.

Wang G, Zhu X, Liang S, Xu F, Liang D and Zeng C (2025). Optimizing preparation of renal biopsy specimens for TEM: A time-efficient approach to rapid diagnosis of kidney diseases. *Ren Fail,* **47**(1): 2522325.

Xu Z, Yang S, Tan Y, Zhang Q, Wang H, Tao J, Liu Q, Wang Q, Feng W, Li Z, Wang C and Cui L (2025). Inflammation in cardiovascular-kidney-metabolic syndrome: Key roles and underlying mechanisms-a comprehensive review. *Mol Cell Biochem,* **480**: 6039-6075.

Yan J, Zhang Z, Yang J, Mitch WE and Wang Y (2015). JAK3/STAT6 stimulates bone marrow-derived fibroblast activation in renal fibrosis. *J Am Soc Nephrol,* **26**: 3060-71.

Zhang Y, He D, Zhang W, Xing Y, Guo Y, Wang F, Jia J, Yan T, Liu Y and Lin S (2020). ACE inhibitor benefit to kidney and cardiovascular outcomes for patients with non-dialysis chronic kidney disease stages 3-5: A network meta-analysis of randomised clinical trials. *Drugs,* **80**: 797-811.

Zhao W, Liu L, Wang Y, Mao T and Li J (2016). Effects of a combination of puerarin, baicalin and berberine on the expression of proliferator-activated receptor-γ and insulin receptor in a rat model of nonalcoholic fatty liver disease. *Exp Ther Med,* **11**: 183-190.

Zhu M, Wei R, Yuan B, Li S and Hu F (2025). Integrated transcriptomics and network pharmacology reveal the mechanism of poplar-type propolis on the mouse mastitis model. *Nutrients,* **17**(23): 3683.